JPEDAV (2010) 31:439–444
DOI: 10.1007/s11669-010-9782-9
1547-7037 ©ASM International

New Contribution to the Thermodynamics of Fe-Cr Alloys as Base for Ferritic Steels

G. Bonny, D. Terentyev, and L. Malerba

(Submitted May 3, 2010; in revised form July 1, 2010)

High chromium ferritic-martensitic steels are commonly used for industrial applications requiring high strength at elevated temperature. Such steels typically contain 9-14 at.% Cr and a few percents of minor alloying elements. In recent studies it has been shown that the Cr solubility limit of the standard Fe-Cr phase diagram in that composition range is significantly underestimated. For the purpose of more reliable engineering and out of physical considerations, we reparameterize the Gibbs free energy so that the correct Cr solubility at low temperature (< 700 K) is reproduced, while leaving the rest of the phase diagram changed only slightly. The mixing enthalpy and heat capacity resulting from the new parameterization are also compared with experiments and found to be in good agreement.

Keywords CALPHAD approach, Fe-Cr system, phase diagram, thermodynamic modeling

1. Introduction

The Fe-Cr phase diagram published in handbooks[1,2] shows the existence of four stable solid phases, namely: the body-centred-cubic (bcc) α and α', respectively rich in iron and in chromium; the face-centred-cubic (fcc) γ, which is confined to a closed region between ~1100 and 1700 K and limited to Cr concentrations, x_{Cr}, up to ~12 at.% (henceforth %)—the so-called γ-loop; and the complex σ-phase, confined around $x_{Cr} \sim 50\%$ and above temperatures between ~800 and 1100 K. These phases coexist in different regions: below ~800 K there is a miscibility gap between α and α', which becomes metastable above this temperature and at equilibrium divides up into the α-σ and σ-α' regions; in the thin region delimiting the γ-loop, on the other hand, the α and γ phases co-exist. All the rest of the diagram corresponds to a single bcc phase, which is limited by the liquid-solid phase equilibria at very high temperature. This phase diagram is well reproduced by the CALPHAD formulation proposed by Andersson and Sundman[3] (henceforth standard parameterization). The latter is based on experimental data above 700 K and for alloys with $x_{Cr} > 10\%$, but has been shown to appreciably underestimate the Cr solubility below it.[4,5]

The region of Cr concentration around 10% is of special interest for power industry applications at elevated temperature (up to 920 K). As a matter of fact, ferritic-martensitic (FM) steels containing up to 12% Cr have been historically developed to provide high resistance to creep.[6] The addition of 1-2.5% Cr to Mo-alloyed steels doubles the 100,000 h creep rupture strength at 770 K (from 70 to 140 MPa). However, in order to obtain acceptable 100,000 h creep rupture strength (~100 MPa) up to 870 K, a higher Cr content is required and the best performances have been achieved with x_{Cr} between 9 and 12%.

Because of these good high temperature properties, combined with higher thermal conductivity and lower expansion coefficient than austenitic steels, 9-12% Cr FM steels have also been chosen since the 1970s as candidate structural materials for future nuclear reactors, such as Generation IV concepts and fusion systems.[7,8] An additional reason to use these materials for nuclear applications is that experimental studies of their behavior under neutron irradiation showed that they are much less affected by irradiation swelling than austenitic steels.[7,8] Thus, commercial and experimental FM steels containing about 9-12% Cr and few percents of minor alloying elements have been considered or developed for nuclear applications in Russia, the US, Japan, China, and Europe.[9,10] As an illustration, the typical composition of some of these high-Cr steels is summarized in Table 1.

The target in the power industry, both nuclear and non-nuclear, is to work at high temperatures in order to increase thermal efficiency and, more recently, reduce carbon dioxide emissions. However, the material will, in practice, be exposed to temperatures ranging from ambient to the maximum acceptable by design. The case of liquid-metal-cooled nuclear reactors is especially critical, because the materials will spend long times during maintenance at temperatures that must be high enough to keep the metal liquid. These temperatures correspond to those for which the Fe-Cr standard phase diagram is not correct, by predicting a much lower solubility of Cr in Fe than the real one.[4,5] The actual position of the solubility limit then becomes critical because, if the material happens to be inside the α-α' miscibility gap, the supersaturation of point-defects produced by irradiation will rapidly lead to phase separation,[11-13]

G. Bonny, D. Terentyev, and **L. Malerba**, SCK·CEN, Nuclear Materials Science Institute, Boeretang 200, 2400 Mol, Belgium. Contact e-mail: gbonny@sckcen.be.

Table 1 Composition (wt.%) of reduced activation FM steels with a favorable combination of physical properties[9,10]

Country	Name	C	Si	Mn	Cr	W	V	Ta	N	B
Europe	EUROFER	0.1	0.05	0.5	**8-9**	~1	0.2	0.06	0.02	0.004
Europe	OPTIFER	0.1	0.04	0.5	**9.4**	…	0.25		0.015	0.006
Japan	F82H	0.1	0.2	0.5	**8**	~2	0.2	0.04	<0.01	0.003
Japan	JLF-1	0.1	0.08	0.045	**9.0**	2.0	0.2	0.07	0.05	0.006
USA	ORNL(9Cr-2WVTa)	0.1	0.3	0.4	**9**	~2	0.25	0.07	…	…
USA	HT9(12Cr-1MoWV)	0.2	0.4	0.6	**12.0**	1.0	0.5	0.25	…	…
Russia	EP-823	0.18	1.05	0.6	**11.4**	0.65	0.4	…	0.04	0.004
Russia	EP-450	0.1	0.18	0.32	**13**	0.65	0.28	…	0.04	0.04
China	CLAM	0.11	0.01	0.4	**8.98**	1.55	0.21	0.15	0.02	…

Cr content is highlighted in bold

subsequently causing unwanted embrittlement.[14-18] The steel compositions considered for nuclear applications are exactly in the region where the solubility limit is expected to be, therefore small composition variations will determine whether or not the material will be susceptible to embrittlement during operation. It should be noted that in actual steels carbon content and heat treatment have a significant influence on the micro-structure of high-Cr steels. In addition, carbon also influences the equilibrium phase diagram.[19] The present work, however, is limited to the equilibrium phase diagram of the binary Fe-Cr system.

The physical explanation for the higher solubility limit than predicted by the standard phase diagram is the existence of a tendency for Cr atoms to produce short-range order (SRO) in Fe which has been experimentally observed[20-22] and is also supported by both theoretical considerations[23] and density functional theory (DFT) calculations,[24-30] which predict a negative heat of mixing (HOM) below about 10% Cr. However, the standard Calphad parameterization does not account for this at all. Thus, it appears necessary to re-parameterize the equations describing the thermodynamic properties of the Fe-Cr system, as predicted by the standard parameterization, so as to re-adjust the low temperature Fe-rich phase boundary. In this work a new parameterization of the Gibbs free energy for the bcc phase is proposed, based on theoretical considerations and the newly proposed Fe-rich phase boundary.[4] The re-parameterized free energy surface is merged smoothly with the standard parameterization at 1100 K, so that the thermodynamic properties above this temperature remain unchanged. The γ-loop and the liquid-solid equilibrium are beyond the scope of the present work.

2. Thermodynamic Model

The sub-regular solution model used in the standard parameterization has proven unable to reproduce the change of sign in the mixing enthalpy and the high Cr solubility below 700 K. Since a sub-lattice model seems to be inappropriate to describe the effects of SRO, a solution model including higher order interactions in composition (here up to fifth order) is used.[31]

The total molar Gibbs free energy $G_{\mathrm{tot}}^{\mathrm{bcc}}$ is given as,

$$G_{\mathrm{tot}}^{\mathrm{bcc}} = x_{\mathrm{Cr}} G_{\mathrm{Cr}}^{\mathrm{bcc}} + x_{\mathrm{Fe}} G_{\mathrm{Fe}}^{\mathrm{bcc}} + RT(x_{\mathrm{Cr}} \ln x_{\mathrm{Cr}} + x_{\mathrm{Fe}} \ln x_{\mathrm{Fe}}) + G_{\mathrm{xc}}^{\mathrm{bcc}} + G_{\mathrm{M}}^{\mathrm{bcc}}. \qquad \text{(Eq 1)}$$

Here the first two terms give the contribution from the mechanical mixture, the third one is the contribution from the configurational entropy for an ideal solution,[32] the fourth term describes concentration dependent interactions and the last term accounts for the magnetic contribution to the free energy. In addition, in Eq 1, x_{Cr} (x_{Fe}) denotes the molar fraction of Cr(Fe), R denotes the gas constant and T is the absolute temperature.

The free energy of the pure elements, $G_{\mathrm{Fe}}^{\mathrm{bcc}}$ and $G_{\mathrm{Cr}}^{\mathrm{bcc}}$ is taken from the SGTE (Scientific Group Thermodata Europe) database[33] and is given in the Appendix. The excess free energy is expressed as a Redlich-Kister polynomial,[34]

$$G_{\mathrm{xc}}^{\mathrm{bcc}} = x_{\mathrm{Fe}} x_{\mathrm{Cr}} \sum_{p=0}^{N} L_p^{\mathrm{bcc}}(T)(x_{\mathrm{Cr}} - x_{\mathrm{Fe}})^p, \qquad \text{(Eq 2)}$$

with N being the order of the composition dependent interaction (here $N = 5$) and L_p^{bcc}(T) the p-th interaction parameter between Cr and Fe, given as,

$$L_p^{\mathrm{bcc}}(T) = l_0^p + l_1^p T + l_2^p T^2 + l_3^p T^3. \qquad \text{(Eq 3)}$$

The magnetic term, $G_{\mathrm{M}}^{\mathrm{bcc}}$, has been defined by Hillert and Jarl[35] following the work of Inden[36,37] and is given in the Appendix.

3. Parameterization

The optimization of the Gibbs free energy parameters $\{l_0^p, \ldots, l_3^p\}$ was performed in the temperature range 298.15-1100 K. The six parameters $\{l_0^0, \ldots, l_0^5\}$ were optimized to reproduce the new Fe-rich phase boundary, the standard Cr-rich phase boundary and the DFT calculated mixing enthalpy.[28] For each trial set $\{l_0^0, \ldots, l_0^5\}$ the other parameters were determined by the constraints of continuity of Gibbs free energy surface, enthalpy surface, entropy surface and heat capacity in T at all compositions with requirement to blend into the standard parameterization at 1100 K. The latter constraint translates to,

$$\left.\frac{\partial^n G_{\mathrm{xc}}^{\mathrm{new}}}{\partial T^n}\right|_{T=1100} = \left.\frac{\partial^n G_{\mathrm{xc}}^{\mathrm{standard}}}{\partial T^n}\right|_{T=1100}, \qquad \text{(Eq 4)}$$

for n = 0, 1, 2 and thus uniquely determine the remaining parameters. Note that the temperature 1100 K falls just below the onset of the γ-loop, which starts at 1120 K, so by definition the position of the γ-loop and liquid-solid phase boundaries remains unchanged. The obtained parameters are summarized in the Appendix.

4. Results and Discussion

The metastable miscibility gap resulting from the new parameterization for the free energy is presented in Fig. 1. In the same figure, the miscibility gap obtained from the standard parameterization is plotted together with the new Fe-rich phase boundary. The new parameterization does not provide an exact fit to the boundary suggested by Bonny et al.,[4] but this is not necessary since the suggested boundary is only indicative. The boundary resulting from the new parameterization, however, does reproduce a large solubility of Cr (~7% Cr) at low temperature (<700 K). Aside from the Fe-rich phase boundary below 700 K, the miscibility gap is almost coincident with the standard one. A comparison of the equilibrium bcc-σ-phases, obtained with the two parameter sets, shows that the phase boundaries are almost coincident. The reason for this lays in the smooth transition of the re-assessed free energy surface with the original one, as explained above. For completeness, we mention that the isotherm at the onset of σ-phase formation is shifted up by 7 K compared to the standard parameterization and that above 750 K the difference in the location of any phase boundary between new and standard parameterization is at most 2%.

Figure 2 compares the mixing enthalpy at 900 K for the two sets of parameters. Both curves are almost coincident and have a parabolic shape in agreement with experimental observations in the paramagnetic bcc phase,[38] superposed in Fig. 2. The negative HOM at the Fe-rich side has disappeared as the Curie temperature is approached.

The mixing enthalpy of bcc Fe-Cr solution, calculated at 300 K using the new and standard parameter sets, is presented in Fig. 3, together with the data obtained from the DFT calculations[28] (strictly speaking valid only at 0 K for a random alloy). The shape of the mixing enthalpy reproduced by the proposed parameterization set is in good agreement with the DFT curve, and falls well within the error of the different DFT approaches for $x_{\mathrm{Cr}} > 0.2$ (for a detailed discussion and spread of DFT data[28,39]). For $x_{\mathrm{Cr}} < 0.2$ the minimum value is about double the DFT one as is the value of the zero of the curve. This discrepancy is due to the appearance of SRO in Fe-rich Fe-Cr alloys,[20,21]

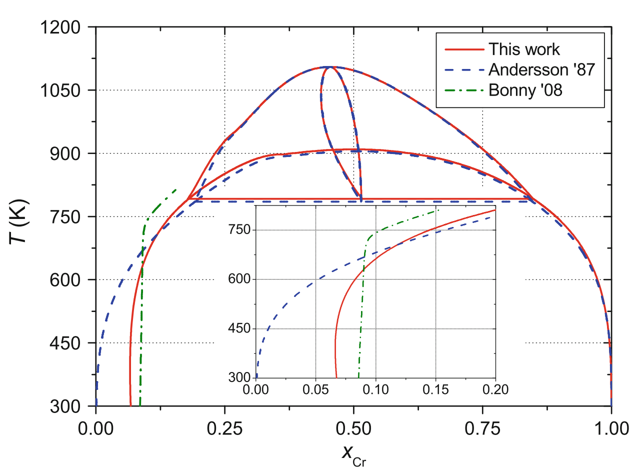

Fig. 1 Calculated metastable miscibility gap

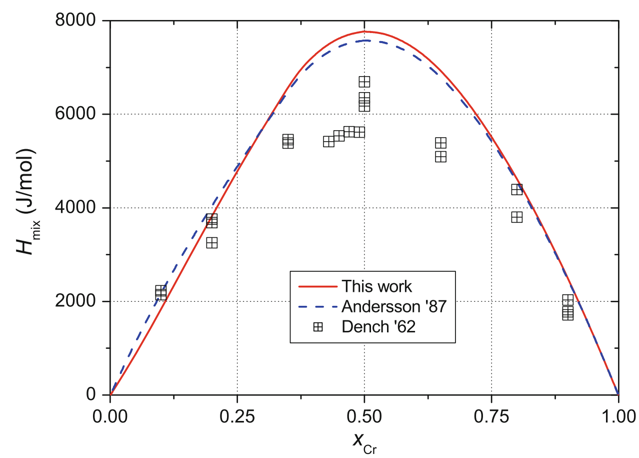

Fig. 2 Mixing enthalpy at 900 K

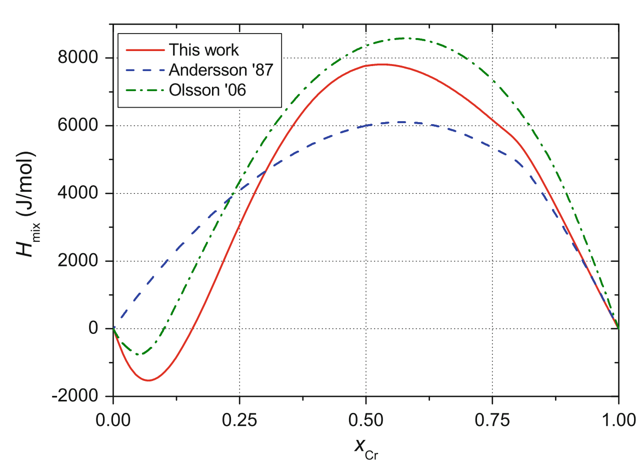

Fig. 3 Mixing enthalpy at 300 K

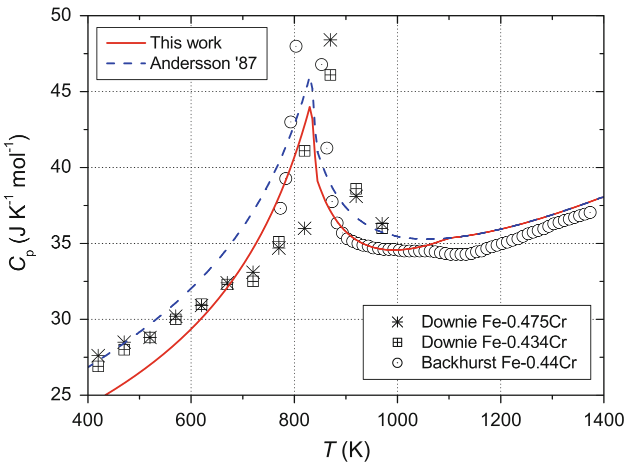

Fig. 4 Heat capacity as a function of temperature

as previously explained.[40] The presence of SRO in the alloy has a negligible effect on the configurational entropy as compared to the random solution, which justifies the use of the ideal solution expression. However, the SRO has a significant impact on the mixing enthalpy, lowering its minimum and shifting it to the Cr-rich side. Keeping in mind that the DFT obtained mixing enthalpy was calculated for random Fe-Cr alloys, the discrepancy can thus be rationalized. The mixing enthalpy obtained from the standard parameterization does not show any change of sign in the whole concentration range and therefore excludes occurrence of SRO, which is also the reason for the low solubility of Cr at temperatures below 700 K predicted by the standard parameterization.

In Fig. 4, the heat capacity, C_p, obtained from the two parameter sets is compared for Fe-0.44Cr in the bcc phase. The two curves are in close agreement and provide the same critical temperature at which the cusp occurs. Note that both calculated curves are also in reasonable agreement with experimental data,[41,42] although such data was not used in the parameterization procedure of either set.

Finally, we emphasize that the use of a high order polynomial in x_{Cr} and T to describe $G_{\mathrm{xc}}^{\mathrm{bcc}}$ did not introduce uncontrolled unnatural oscillations in the thermodynamic function, as illustrated in Figs. 2-4, respectively.

5. Conclusions

Thermodynamic functions of the bcc phase of Fe-Cr alloys were re-parameterized so as (i) to account for the large solubility of Cr in Fe below 700 K, as suggested by Bonny et al.[4] and (ii) to keep the rest of the phase diagram almost coincident. The mixing enthalpy, calculated with the new parameter set, agrees reasonably with existing DFT data, which provide the physical reason for the high solubility of Cr at low temperature. The higher order derivatives of the Gibbs free energy, such as the heat capacity, were proven to be virtually unaffected by the new parameterization and, at the same time, were found to agree with available experimental results.

Acknowledgments

The authors gratefully acknowledge fruitful discussions with Profs. R. C. Pasianot, P. A. Korzhavyi and G. Inden during the preparation of this manuscript. This research has received partial funding from the European Atomic Energy Community's 7th Framework Programme (FP7/2007-2011), under grant agreement number 212175 (GetMat project). The results also contribute to the European Fusion Programme coordinated by the EFDA Fusion Materials Topical Group. Thermo-Calc Software is acknowledged for providing a free data assessment licence of their software.

6. Appendix: Summary of the Parameters

All parameters are given in SI units.

$$
\begin{aligned}
G_{\mathrm{Cr}}^{\mathrm{bcc}}(T) = & -8856.94 + 157.48T - 26.908T\ln T \\
& + 0.00189435T^2 - 1.47721 \times 10^{-6}\,T^3 \\
& + 139250\,T^{-1} \quad \text{for } T \le 2180 \\
= & -34869.344 + 344.18\,T - 50\,T\ln T \\
& - 2.885261 \times 10^{32}T^{-9} \quad \text{for } T > 2180
\end{aligned}
$$

$$
\begin{aligned}
G_{\mathrm{Fe}}^{\mathrm{bcc}}(T) = & \ 1225.7 + 124.134T - 23.5143T\ln T \\
& - 0.00439752T^2 - 5.8927 \times 10^{-8}T^3 \\
& + 77359T^{-1} \quad \text{for } T \le 1811 \\
= & -25383.581 + 299.31255T - 46T\ln T \\
& + 2.296031 \times 10^{31}T^{-9} \quad \text{for } T > 1811
\end{aligned}
$$

$$
\begin{aligned}
L_0^{\mathrm{bcc}}(T) = & \ 29115.4073988 - 33.17656563T \\
& + 0.2136051421 \times 10^{-1}T^2 \\
& - 0.6472883095 \times 10^{-5}T^3 \quad \text{for } T \le 1100 \\
= & \ 20500 - 9.68T \quad \text{for } T > 1100
\end{aligned}
$$

$$
\begin{aligned}
L_1^{\mathrm{bcc}}(T) = & \ 431.304715913 - 1.176285589T \\
& + 0.1069350535 \times 10^{-2}T^2 \\
& - 0.3240456168 \times 10^{-6}T^3 \quad \text{for } T \le 1100 \\
= & \ 0 \quad \text{for } T > 1100
\end{aligned}
$$

$$
\begin{aligned}
L_2^{\mathrm{bcc}}(T) = & -31452.7844978 + 85.78032136T \\
& - 0.7798211033 \times 10^{-1}T^2 \\
& + 0.2363094252 \times 10^{-4}T^3 \quad \text{for } T \le 1100 \\
= & \ 0 \quad \text{for } T > 1100
\end{aligned}
$$

$$L_3^{\mathrm{bcc}}(T) = 48134.0406455 - 131.2746563T + 0.1193405966T^2 - 0.3616381716 \times 10^{-4}T^3 \quad \text{for } T \leq 1100$$
$$= 0 \quad \text{for } T > 1100$$

$$L_4^{\mathrm{bcc}}(T) = -23569.1128794 + 64.27939876T - 0.5843581706 \times 10^{-1}T^2 + 0.1770782335 \times 10^{-4}T^3 \quad \text{for } T \leq 1100$$
$$= 0 \quad \text{for } T > 1100$$

$$L_5^{\mathrm{bcc}}(T) = -5625.73982982 + 15.34292681T - 0.1394811528 \times 10^{-1}T^2 + 0.4226701600 \times 10^{-5}\,T^3 \quad \text{for } T \leq 1100$$
$$= 0 \quad \text{for } T > 1100$$

$$G_{\mathrm{M}}^{\mathrm{bcc}} = RT\,\ln(B_0 + 1)f(T/T_{\mathrm{C}})$$

$$f(\tau) = 1 - 0.9053\tau^{-1} - 0.153\tau^3 - 6.8 \times 10^{-3}\tau^9 - 1.53 \times 10^{-3}\tau^{15} \quad \text{for } \tau \leq 1$$
$$= -6.417 \times 10^{-2}\tau^{-5} - 2.037 \times 10^{-3}\tau^{-15} - 4.278 \times 10^{-4}\tau^{-25} \quad \text{for } \tau > 1$$

$$B_0 = 2.22x_{\mathrm{Fe}} - 0.008x_{\mathrm{Cr}} - 0.85x_{\mathrm{Fe}}x_{\mathrm{Cr}}$$

$$T_{\mathrm{C}} = 1043x_{\mathrm{Fe}} - 311.15x_{\mathrm{Cr}} + x_{\mathrm{Fe}}x_{\mathrm{Cr}}[1650 + 550(x_{\mathrm{Cr}} - x_{\mathrm{Fe}})]$$

Note that when the calculated Curie temperature T_{C} is less than zero, the value should be multiplied by -1 to obtain the experimental Neel temperature.

References

1. R. Hultgren, P.D. Desai, D.T. Hawkins, M. Gleiser, and K.K. Kelley, *Selected Values of the Thermodynamic Properties of Binary Alloys*, AMS, Ohio, 1973
2. T.B. Massalsky, H. Okamoto, P.R. Subramanian, and L. Kacprzac, *Binary Alloy Phase Diagrams*, ASM International, Materials Park, OH, 1990, p 1273
3. J.-O. Andersson and B. Sundman, Thermodynamic Properties of the Cr-Fe System, *CALPHAD*, 1987, **11**, p 83-92
4. G. Bonny, D. Terentyev, and L. Malerba, On the α-α′ Miscibility Gap of Fe-Cr Alloys, *Scr. Mater.*, 2008, **59**, p 1193-1196
5. F. Bergner, A. Ulbricht, and C. Heintze, Estimation of the Solubility Limit of Cr in Fe at 300 °C from Small-Angle Neutron Scattering in Neutron-Irradiated Fe-Cr alloys, *Scr. Mater.*, 2009, **61**, p 1060-1163
6. K.-H. Mayer and F. Masuyama, The Development of Creep-Resistant Steels, *Creep-Resistant Steels*, Vol 2, F. Abe and T.-U. Kern, Ed., Woodhead Publishing Ltd., Abingdon, UK, 2008
7. L.K. Mansur, A.F. Rowcliffe, R.K. Nanstad, S.J. Zinkle, W.R. Corwin, and R.E. Stoller, Materials Needs for Fusion, Generation IV Fission Reactors and Spallation Neutron Sources—Similarities and Differences, *J. Nucl. Mater.*, 2004, **329-333**, p 166-172
8. R.L. Klueh and A.T. Nelson, Ferritic/Martensitic Steels for Next-Generation Reactors, *J. Nucl. Mater.*, 2007, **371**, p 37-52
9. R. Klueh and D. Harries, *High-Chromium Ferritic and Martensitic Steels for Nuclear Applications*, ASTM International, 2001, p 337
10. J. Yu, Q. Huang, and F. Wan, Research and Development on the China Low Activation Martensitic Steel (CLAM), *J. Nucl. Mater.*, 2007, **367-370**, p 97-101
11. F. Bley, Neutron Small-Angle Scattering Study of Unmixing in Fe-Cr Alloys, *Acta Metall. Mater*, 1992, **40**, p 1505-1517
12. P. Dubuisson, D. Gilbon, and J.L. Séran, Microstructural Evolution of Ferritic-Martensitic Irradiated in the Fast Breeder Reactor Phénix, *J. Nucl. Mater.*, 1993, **205**, p 178-189
13. M.H. Mathon, Y. de Carlan, G. Geoffroy, X. Averty, A. Alamo, and C.H. de Novion, A SANS Investigation of the Irradition-Enhanced α-α′ Phases Separation in 7-12 Cr Martensitic Steels, *J. Nucl. Mater.*, 2003, **312**, p 236-248
14. R.M. Fisher, E.J. Dulis, and K.G. Carroll, Identification of the Precipitate Accompanying 885 °F Embrittlement in Chromium Steels, *Trans. AIME*, 1953, **197**, p 690-695
15. R.O. Williams and H.W. Paxton, The Nature of Ageing of Binary Iron-Chromium Alloys Around 500°C, *J. Iron Steel Inst.*, 1957, **185**, p 358-374
16. R. Lagneborg, Metallography of the 475 °C Embrittlement in an Iron-30% Chromium Alloy, *Trans. ASM*, 1967, **60**, p 67-78
17. P.J. Grobner, 885 Degrees F (475 Degrees C) Embrittlement of Ferritic Stainless-Steels, *Metall. Trans.*, 1973, **4**, p 251-260
18. P. Jacobsson, Y. Bergström, and B. Aronsson, Kinetics and Hardening Mechanism of 475 Degrees C Embrittlement in 18Cr-2Mo Ferritic Steels, *Metall. Trans. A*, 1975, **6**, p 1577-1580
19. R.W.K. Honeycombe, *Steels Microstructure and Properties*, Edward Arnold (Publishers) Ltd., London, UK, 1981
20. I. Mirebeau, M. Hennion, and G. Parette, First Measurement of Short-Range-Order Inversion as a Function of Concentration in a Transition Alloy, *Phys. Rev. Lett.*, 1984, **53**, p 687-690
21. N.P. Filippova, V.A. Shabashov, and A.L. Nikolaev, Mössbauer Study of Irradiation-Accelerated Short-Range Ordering in Binary Fe-Cr Alloys, *Phys. Met. Metall.*, 2000, **90**, p 145-152
22. V.V. Sagaradze, I.I. Kositsyna, V.L. Arbuzov, V.A. Shabashov, and Yu.I. Filippov, Phase Transformations in Fe-Cr Alloys upon Thermal Aging and Electron Irradiation, *The Physics of Metals and Metallography*, 2001, **92**, p 508-517
23. M. Hennion, Chemical SRO Effects in Ferromagnetic Fe Alloys in Relation to Electronic Band-Structure, *J. Phys. F*, 1983, **13**, p 2351-2358
24. P. Olsson, I.A. Abrikosov, L. Vitos, and J. Wallenius, Ab Initio Formation Energies of Fe-Cr Alloys, *J. Nucl. Mater.*, 2003, **321**, p 84-90
25. W.T. Geng, Cr Segregation at the Fe-Cr Surface: A First-Principles GGA Investigation, *Phys. Rev. B*, 2003, **68**, p 233402
26. A.A. Mirzoev, M.M. Yalalov, and D.A. Mirzaev, Calculation of the Energy of Mixing for the Fe-Cr Alloys by the First-Principles Methods of Computer Simulation, *Phys. Met. Metall.*, 2004, **97**, p 336-341
27. T.P.C. Klaver, R. Drautz, and M.W. Finnis, Magnetism and Thermodynamics of Defect-Free Fe-Cr Alloys, *Phys. Rev. B*, 2006, **74**, p 094435

28. P. Olsson, I.A. Abrikosov, and J. Wallenius, Electronic Origin of the Anomalous Stability of Fe-Rich Bcc Fe-Cr Alloys, *Phys. Rev. B*, 2006, **73**, p 104416
29. M.Yu. Lavrentiev, R. Drautz, D. Nguyen-Manh, T.P.C. Klaver, and S.L. Dudarev, Monte Carlo Study of Thermodynamic Properties and Clustering in the Bcc Fe-Cr System, *Phys. Rev. B*, 2007, **75**, p 014208
30. P. Olsson, C. Domain, and J. Wallenius, Ab Initio Study of Cr Interactions with Point Defects in Bcc Fe, *Phys. Rev. B*, 2007, **75**, p 014110
31. N. Saunders and A.P. Miodownik, *CALPHAD Calculation of Phase Diagrams, A Comprehensive Guide*, Pergamon, 1998
32. R.T. DeHoff, *Thermodynamics in Materials Science*, 2nd ed., CRC Press, 2006
33. A.T. Dinsdale, SGTE Data for Pure Elements, *CALPHAD*, 1991, **15**, p 317-425
34. O. Redlich and A. Kister, Algebraic Representation of Thermodynamic Properties and the Classification of Solutions, *Ind. Eng. Chem*, 1948, **40**, p 345-348
35. M. Hillert and M. Jarl, Model for Alloying Effects in Ferromagnetic Metals, *CALPHAD*, 1978, **2**, p 227-238
36. G. Inden, *Proc. CALPHAD Conference*, Vol III, Dusseldorf, 1976, p 4
37. G. Inden, The Role of Magnetism in the Calculation of Phase Diagrams, *Physica B*, 1981, **103**, p 82-100
38. W.A. Dench, Adiabatic High-Temperature Calorimeter for the Measurement of Heats of Alloying, *Trans. Faraday Soc.*, 1963, **59**, p 1279-1292
39. G. Bonny, R.C. Pasianot, L. Malerba, A. Caro, P. Olsson, and M.Yu. Lavrentiev, Numerical Prediction of Thermodynamic Properties of Iron-Chromium Alloys Using Semi-Empirical Cohesive Models: The State of the Art, *J. Nucl. Mater.*, 2009, **385**, p 268-277
40. G. Bonny, P. Erhart, A. Caro, R.C. Pasianot, L. Malerba, and M. Caro, The Influence of Short Range Order on the Thermodynamics of Fe-Cr Alloys, *Model. Simul. Mater. Sci. Eng.*, 2009, **17**, p 025006
41. I. Backhurst, The Adiabatic Vacuum Calorimeter from 600 to 1600 °C, *J. Iron Steel Inst.*, 1958, **189**, p 124-134
42. D.B. Downie and J.F. Martin, Heat-Capacities of Transition-Metal Alloys 2. Alpha- and Sigma-Phase $Fe_{0.525}Cr_{0.475}$ and $Fe_{0.566}Cr_{0.434}$, *J. Chem. Thermodyn.*, 1984, **16**, p 743-752